BMO TR-81-77

SAI DOCUMENT NO. SAI-067-82R-006

PERFORMANCE TECHNOLOGY PROGRAM (PTP-S II)

VOLUME XIV

EXTENSIONS TO THE 3DSAP APPROXIMATE INVISCID FLOW FIELD CODE

SCIENCE APPLICATIONS, INC.
APPLIED MECHANICS OPERATION
WAYNE, PENNSYLVANIA 19087

FEBRUARY, 1981

FINAL REPORT FOR PERIOD SEPTEMBER 1980 - FEBRUARY 1981

CONTRACT NO. F04701-77-C-0126

AIR FORCE BALLISTIC MISSILE OFFICE
NORTON AIR FORCE BASE, CALIFORNIA 92409

This final report was submitted by Science Applications, Inc., 1200 Prospect Street, La Jolla, California 92038, under Contract Number F04701-77-C-0126 with the Ballistic Missile Office, AFSC, Norton AFB, California. Major Kevin E. Yelmgren, BMO/SYDT, was the Project Officer in charge. This technical report has been reviewed and is approved for publication.

Kevin E. Yelmgren

KEVIN E. YELMGREN, Major, USAF
Chief, Vehicle Technology Branch
Reentry Technology Division
Advanced Ballistic Reentry Systems

FOR THE COMMANDER

Nicholas C. Belmonte

NICHOLAS C. BELMONTE, Lt Col, USAF
Director, Reentry Technology Division
Advanced BAllistic Reentry Systems

UNCLASSIFIED

SECURITY CLASSIFICATION OF THIS PAGE (When Data Entered)

REPORT DOCUMENTATION PAGE		READ INSTRUCTIONS BEFORE COMPLETING FORM
1. REPORT NUMBER BMO-TR-81-77	2. GOVT ACCESSION NO. AD-A102 858	3. RECIPIENT'S CATALOG NUMBER
4. TITLE (and Subtitle) PERFORMANCE TECHNOLOGY PROGRAM (PTP-S II); VOL. XIV. EXTENSIONS TO THE 3DSAP APPROXIMATE INVISCID FLOW FIELD CODE		5. TYPE OF REPORT & PERIOD COVERED FINAL REPORT, 9/80 - 2/81 6. PERFORMING ORG. REPORT NUMBER SAI-067-82R-006
7. AUTHOR(s) Darryl W. Hall Catherine M. Dougherty		8. CONTRACT OR GRANT NUMBER(s) F04701-77-C-0126
9. PERFORMING ORGANIZATION NAME AND ADDRESS Science Applications, Inc. 994 Old Eagle School Rd., Suite 1018 Wayne, Pennsylvania 19087		10. PROGRAM ELEMENT, PROJECT, TASK AREA & WORK UNIT NUMBERS Task 3.2.1.9.2
11. CONTROLLING OFFICE NAME AND ADDRESS BMO/SYDT Norton Air Force Base, California		12. REPORT DATE February 1981 13. NUMBER OF PAGES 52
14. MONITORING AGENCY NAME & ADDRESS(if different from Controlling Office)		15. SECURITY CLASS. (of this report) Unclassified 15a. DECLASSIFICATION/DOWNGRADING SCHEDULE

16. DISTRIBUTION STATEMENT (of this Report)

Approved for public release; distribution unlimited.
Distribution Statement "A" of AFR 80-45 applies.

17. DISTRIBUTION STATEMENT (of the abstract entered in Block 20, if different from Report)

18. SUPPLEMENTARY NOTES

19. KEY WORDS (Continue on reverse side if necessary and identify by block number)

Flow Fields
Aerodynamics
Reentry Vehicles
Asymmetric Nosetips
Flared Bodies
Hypersonic Flow

20. ABSTRACT (Continue on reverse side if necessary and identify by block number)

The 3DSAP approximate inviscid flow field technique has been modified to permit treatment of flared multi-conic afterbodies. The calculation of the flared afterbody section is performed using a discrete shock-fitting algorithm to accurately treat the embedded shock. Additional modifications have been incorporated into the code, allowing stretching of the body-normal coordinate grid and improving the treatment of expansion discontinuities on the multi-conic frustum.

DD FORM (FACSIMILE) 1473

AD-A102 858

UNCLASSIFIED

SECURITY CLASSIFICATION OF THIS PAGE (When Data Entered)

TABLE OF CONTENTS

LIST OF FIGURES

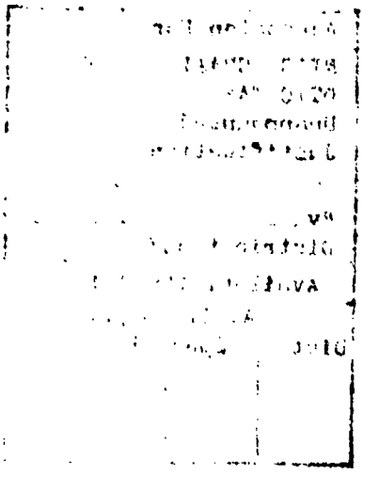

NOMENCLATURE

a	Isentropic speed of sound
h	Static enthalpy
H	Ratio of local coordinate system curvature to body radius of curvature, $1 + y/R$
H_∞	Total (stagnation) enthalpy, $h + 1/2q^2$
K	Curvature of body
M	Mach number
p	Pressure
P	Logarithm of pressure
q	Total velocity, $\sqrt{u^2+v^2+w^2}$
r	Radial coordinate in cylindrical coordinates
$\hat{r}$	Cross-section radius
R	Body radius of curvature, or gas constant
s	Entropy
T	Temperature
u	Tangential velocity component in body-normal coordinates
v	Normal velocity component in body-normal coordinates
V_∞	Freestream velocity
w	Circumferential velocity component in body-normal coordinates
x	Wetted length, measured along body surface from stagnation point
y	Distance from body surface, measured along body-normal
z	Axial coordinate in cylindrical coordinates

NOMENCLATURE (Cont'd.)

α	Angle of attack
α^*	Stretching parameter
β	Sideslip angle
γ	Isentropic exponent
ε	Convergence criterion for iterative calculations
η	Transformed normal coordinate
θ	Circumferential coordinate in (ξ,η,θ) coordinates
θ_b	Local body angle
λ	Characteristic slope
ξ	Wetted length in (ξ,η,θ) coordinates
ρ	Density
σ	Normal streamline slope, v/u
σ_s	Local shock slope, $\tan^{-1}\partial r_s/\partial z$
τ	Circumferential streamline slope, w/u
ϕ	Circumferential coordinate
$\hat{\phi}$	Circumferential coordinate (nose geometry)
$(\ )_b$	Condition at body
$(\ )_{EB}$	Equivalent body quantity
$(\ )_s$	Condition at shock
$(\ )_o$	Stagnation point condition
$(\ )_\infty$	Freestream condition
$(\ )_*$	Sonic point condition

SECTION 1

INTRODUCTION

This report describes work performed under Task 3.2.1.9, "Asymmetric Flow Field Modeling," Subtask 3.2.1.9.2, "3DSAP Modifications," of the Performance Technology Program (PTP-S II). This effort involved the extension of the Three-Dimensional Shock and Pressure (3DSAP) approximate inviscid flow field technique to treat flared multi-conic frustum configurations.

The 3DSAP approximate flow field technique was originally developed to provide rapid yet accurate aerodynamic predictions for ballistic reentry vehicles with asymmetric ablated nosetips (References 1 and 2). In 3DSAP the nosetip flow field solution is developed by assigning surface pressures from a correlation and iterating on bow shock position until mass continuity is satisfied, assuming the functional forms of the profiles of the flow properties across the shock layer. The frustum flow field solution is obtained from the finite difference solution of the three-dimensional inviscid flow equations, using initial data from the nosetip flow field solution. The solution of the 3-D inviscid equations on the frustum is simplified by assuming the functional form of the cross-flow distribution and limiting the analysis to small angles of attack and axisymmetric frusta. (As originally developed, the 3DSAP code was restricted to conic or expansion biconic frusta.)

Section 2 of this report describes an optional nosetip pressure correlation that has been added to 3DSAP for use on indented nosetip geometries. This optional correlation was developed in an earlier task of the PTP-S II program for use on indented nosetip geometries in a dispersion code (Reference 3).

The modification of the 3DSAP code to allow radial grid stretching in the supersonic finite difference calculations is described in Section 3. The addition of this option to the code permits the clustering of mesh points near the wall to resolve the flow gradients that may arise there, while retaining the formal second order accuracy of the finite difference procedure used.

In Section 4 the extension of the geometric capabilities of the 3DSAP code to multi-conic axisymmetric afterbodies is described. Included in this new capability is an improved procedure for treating the discontinuities of both the flow and the coordinate system at expansion corners.

Finally, in Section 5, the addition of the capability of treating flared afterbody sections to the 3DSAP code is described. In this analysis it is assumed that there is an attached embedded shock on the flare and that the flow behind the shock remains supersonic. A discrete shock-fitting algorithm has been developed to accurately treat the embedded shock.

The appendices to this report provide a modified user's guide to the 3DSAP code.

SECTION 2

MODIFIED NOSETIP SURFACE PRESSURE CORRELATION

As described in Reference 1, the 3DSAP approximate flow field procedure assigns nosetip surface pressures from correlations, assuming that each meridional plane on the nosetip is treated as an equivalent axisymmetric body. In the original 3DSAP analysis, the approximate location of the sonic point is determined from a correlation relating the sonic point body angle to the inverse bluntness of the nosetip, as developed in Reference 4. In the subsonic region upstream of the sonic point, the surface pressure is assigned from Love's "Newtonian Deficiency Method,"[5] as modified in Reference 4. Downstream of the sonic point, the surface pressure is assigned from a curve fit developed in Reference 4 of a matched Newtonian plus Prandtl-Meyer expansion.

In Reference 3, as part of the PTP-S II program, this surface pressure correlation procedure was modified to provide more accurate results for indented nosetip geometries for application to a ballistic reentry vehicle (BRV) dispersion code. This improved correlation has been incorporated as an option in the 3DSAP code, and is described below.

Using the nomenclature of the original 3DSAP equivalent body analysis (Reference 1), the sonic point body angle is defined as

$$\theta^* = 50^\circ - \alpha_{EQ} \tag{2.1}$$

where the equivalent angle of attack is defined as

$$\alpha_{EQ} = -\alpha \cos \hat{\phi} + \beta \sin \hat{\phi} \quad . \tag{2.2}$$

The wetted length from the stagnation point to the sonic point is denoted by s*, and the local cylindrical radius is r*. The nosetip pressure correlation is applied in two parts: one upstream of the sonic point and the other downstream. Upstream of the sonic point, the correlation consists of a melding of correlations for spheres, cones, and flat-faced disks, including curvature effects for indented shapes.

The spherical pressure correlation, a modification of the form given by Kyriss and Neff[4], is

$$\bar{p}_s = 1 - 1.08 \left(1 - \frac{p_\infty}{p_0}\right) \cos^2 \theta_{b_{EQ}} \tag{2.3}$$

where $\bar{p} = p/p_0$, p_0 is the stagnation pressure, and the equivalent body angle is

$$\theta_{b_{EQ}} = \theta_b + \alpha_{EQ} \quad . \tag{2.4}$$

The conical pressure correlation, which has been developed in Reference 3 to include effects of concave geometries, is given by

$$\bar{p}_c = \min \left\{ 1.0, \left(1.15 \sin^2 \theta_{b_{EQ}} + \delta\right) \times \left(1 - \frac{p_\infty}{p_0}\right) + \frac{p_\infty}{p_0} \right\} \tag{2.5}$$

where the term δ is 0 for convex geometries. For concave geometries, δ accounts for curvature effects by taking the form

$$\delta = \frac{1}{2r} \bar{K} \cos \theta_{b_{EQ}} \left(r^2 - r_i^2\right) \tag{2.6}$$

where r_i is the cylindrical radius at the start of the concave section, and $\bar{K}$ is an average curvature, defined as

$$\bar{K} = \frac{1}{3} \left[\frac{\int_{s_1}^{s} K ds}{s - s_1} + 2K \right] \quad . \tag{2.7}$$

(Here, s_1 is the wetted length at the start of the concave section.) K is the local curvature at a given point.

The spherical and conical pressure correlations are combined with a correlation for flat disks to yield

$$\bar{p} = \bar{R}^3 \left[\bar{p}_s - (\bar{p}_s - \bar{p}_*) f_{FD}\right] + (1 - \bar{R}^3)\left[\bar{p}_c - (\bar{p}_c - \bar{p}_*) f_{FD}\right] \quad (2.8)$$

where, from References 5 and 6,

$$f_{FD} = B(s/s^*)^2 + (1-B)\, e^{-\lambda} \quad (2.9)$$

with

$$B = \frac{1}{16\ (1 - \bar{p}_*)}$$

$$\lambda = 5\sqrt{\ln\ (s^*/s)}$$

$$\bar{p}_* = 0.532$$

The weighting factor, $\bar{R}$, is defined as

$$\bar{R} = \min\ \{1.0,\ -\frac{1}{K_o}\ (\pi/2 - \theta_b)/s\} \quad (2.10)$$

where K_o is the curvature at the stagnation point.

Downstream of the sonic point, the same basic approach is used, except that the spherical pressure correlation is replaced with the curve fit of a matched Newtonian plus Prandtl-Meyer expansion developed by Kyriss and Neff[4]:

$$\bar{p}_s = \left(1 - \frac{p_\infty}{p_o}\right)\left[1 - 1.46143 \sin^2 (\phi_{EQ} + \Delta\theta) + 0.51143 \sin^3 (\phi_{EQ} + \Delta\theta)\right] + \frac{p_\infty}{p_o} \qquad (2.11)$$

where

$$\phi_{EQ} = \frac{\pi}{2} - \theta b_{EQ}$$

$$\Delta\theta = \theta^* - 50^o$$

In addition, the weighting factor $\bar{R}$ is redefined to be

$$\bar{R} = R^* \frac{\frac{\pi}{2} - \theta_b}{s} \qquad (2.12)$$

with $R^* = r^*/\cos\theta^*$. Finally, the conical pressure term, given by Equation (2.5), is constrained to not exceed the term $\bar{p}_s$ given by Equation (2.11), and the resulting pressure is given by

$$\bar{p} = \bar{R}^3 \bar{p}_s + (1 - \bar{R}^3) \bar{p}_c \qquad (2.13)$$

This optional nosetip pressure correlation is invoked automatically by 3DSAP for non-spherical nosetips, or can be selected by the user by setting the input parameter IPRESS to 2. Comparisons of the nosetip surface pressures predicted with this correlation to experimental data for indented nosetips may be found in Reference 3.

SECTION 3

NORMAL GRID STRETCHING FOR SUPERSONIC CALCULATIONS

In the original 3DSAP analysis of Reference 1, supersonic calculations were performed in a computational transformed coordinate system (ξ,η,θ), where the transformed normal coordinate η was defined as

$$\eta = y/y_s\ (x,\phi) \tag{3.1}$$

where y is the coordinate normal to the body surface and $y = y_s\ (x,\phi)$ defines the bow shock surface. With this transformation η varies between 0 at the body and 1 at the bow shock, and computational grid points equally spaced in η are also equally spaced in y along a given line x = constant, ϕ = constant.

To allow for radial grid stretching the coordinate transformation defined by Equation (3.1) has been generalized to the form

$$\eta = f(y/y_s) \quad . \tag{3.2}$$

By a suitable choice of the function f, it is then possible to cluster mesh points near the wall which are equally spaced in the transformed coordinate η (i.e., the mesh points will be unequally spaced in y). Such a transformation will permit the accurate resolution of strong flow gradients near the wall (e.g., entropy layers) while retaining the formal second order accuracy of the integration procedure used, for which mesh points equally spaced in the computational coordinates are required.

The form of the stretching function incorporated into 3DSAP is that developed by Moretti in Reference 7. In this formulation the stretched coordinate η is defined implicitly from

$$y/y_s = 1 + \tanh\ [\alpha^*(\eta-1)]/\tanh\alpha^* \tag{3.3}$$

where α^* is the stretching parameter. The effect of this formulation on the distribution of grid points is shown in Figure 3.1; note that as the stretching parameter approaches zero the effect of the transformation on the grid point distribution diminishes.

With the coordinate stretching defined by Equation (3.3), the transformation of derivatives in the physical (x,y,ϕ) coordinates to the computational (ξ,η,θ) coordinates becomes

$$\frac{\partial}{\partial x} = \frac{\partial}{\partial \xi} + f_x \frac{\partial}{\partial \eta} \tag{3.4}$$

$$\frac{\partial}{\partial y} = f_y \frac{\partial}{\partial \eta} \tag{3.5}$$

$$\frac{\partial}{\partial \phi} = \frac{\partial}{\partial \theta} + f_\phi \frac{\partial}{\partial \eta} \tag{3.6}$$

where

$$f_y = \frac{D}{\alpha^*[D^2-(y-y_s)^2]}$$

$$f_x = f_y \, y_{s_x} \, y/y_s$$

$$f_\phi = f_y \, y_{s_\phi} \, y/y_s$$

$$D = y_s/\tanh \alpha^*$$

Note that as $\alpha^* \to 0$, these forms reduce to

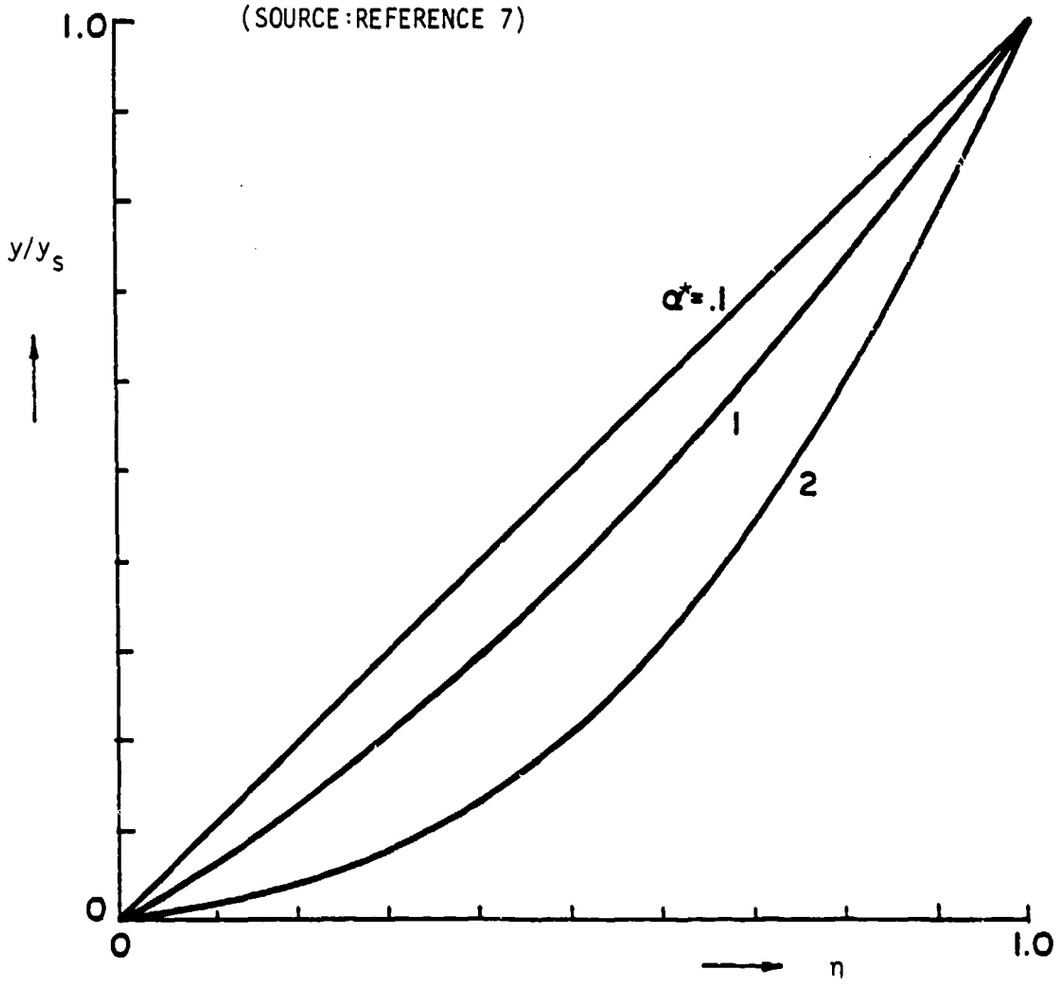

FIGURE 3.1. GRID POINT DISTRIBUTION WITH COORDINATE STRETCHING

$$f_y = \frac{1}{y_s}$$

$$f_x = -\eta\, y_{s_x}/y_s$$

$$f_\phi = -\eta\, y_{s_\phi}/y_s$$

which are the forms given by Equations (2.2.9) - (2.2.11) in Reference 1, in which there is no coordinate stretching.

With coordinate stretching the three-dimensional inviscid equations of motion become, using the nomenclature of Reference 1,

CONTINUITY

$$\left(1 - \frac{a^2}{u^2}\right) P_\xi + \left(A - \frac{a^2}{u^2} f_x\right) P_\eta + B P_\theta + \gamma H \left[f_y \sigma_\eta + \frac{\delta 2}{r}\left(f_\phi \tau_\eta + \tau_\theta + \tau^2 \sin\theta_b\right) + \frac{\delta 1}{r}\left(\sin\theta_b + \sigma\cos\theta_b\right)\right] = 0 \tag{3.7}$$

MOMENTUM

$$\sigma_\xi + A\sigma_\eta + B\sigma_\theta + \frac{P}{\rho u^2}\left[-\sigma P_\xi + \left(Hf_y - \sigma f_x\right) P_\eta\right] - \frac{1+\sigma^2}{R} - \tau B\left(\cos\theta_b - \sigma\sin\theta_b\right) = 0 \tag{3.8}$$

$$\tau_\xi + A\tau_\eta + B\tau_\theta + \frac{P}{\rho u^2}\left[-\tau P_\xi + \left(Hf_\phi/r - \tau f_x\right) P_\eta + \frac{H}{r} P_\theta\right] + B\left(\sin\theta_b + \sigma\cos\theta_b\right) - \frac{\sigma\tau}{R} + \tau^2 B \sin\theta_b = 0 \tag{3.9}$$

ENERGY

$$s_\xi + A s_\eta + B s_\theta = 0 \tag{3.10}$$

where

$$A = f_x + \sigma H f_y + B f_\phi$$

$$B = \delta_2 \tau H / r$$

At body points, the form of the characteristic compatibility equation that is solved with coordinate stretching takes the form

$$P_\xi = -\lambda P_\eta - [BP_\theta + \gamma\{\sigma_\eta f_y + (\delta_2 \tau_\theta + \delta_1 \sin\theta_b)/r + \tau B\left(\sin\theta_b - \frac{f_y \cos\theta_b}{\lambda}\right) - \frac{f_y}{\lambda R}\}]/\left(1 - \frac{a^2}{u^2}\right) \tag{3.11}$$

with

$$\lambda = -f_y / \sqrt{u^2/a^2 - 1}$$

At bow shock points the new characteristic compatibility condition takes the form

$$\frac{aHf_y}{u}\beta_1 (P_\xi + \lambda P_\eta) - \frac{\gamma}{u}(A - f_x)(u_\xi + \lambda u_\eta) + \frac{\gamma H}{u} f_y (v_\xi + \lambda v_\eta) - \sum_{i=1}^{3} \ell_i R_i = 0 \tag{3.12}$$

where

$$\beta_1 = \sqrt{(1 - \frac{a^2}{u^2}) + (\sigma + \frac{\delta 2 \tau}{r} \frac{f_\phi}{f_y})^2}$$

$$\lambda = (A - \frac{a^2}{u^2} f_x + \frac{aHf_y}{u} \beta_1)/(1 - \frac{a^2}{u^2})$$

$$\ell_1 = \lambda - A$$

$$\ell_2 = -\frac{\gamma}{u} (\lambda - f_x)$$

$$\ell_3 = \frac{\gamma H}{u} f_y$$

$$R_1 = -[BP_\theta + \frac{\gamma H}{u} \frac{\delta 2}{r} (w_\theta + f_\phi w_\eta) + \frac{\gamma H \delta 1}{r} (\sin \theta_b + \tau \cos \theta_b) + \frac{\gamma \sigma}{R}]$$

$$R_2 = -[Bu_\theta + \frac{\gamma u}{R} - \tau u B \sin \theta_b]$$

$$R_3 = -[Bv_\theta - \frac{u}{R} - \tau u B \cos \theta_b] \quad .$$

In the modified version of 3DSAP, the Equations (3.7) - (3.12) are solved exactly as were their counterparts without coordinate stretching in the original 3DSAP, with only one small variation. It has recently been noted that in the bow shock point solution procedure, where the bow shock slope is iterated until Equation (3.12) is satisfied to within some tolerance ε, that the equation is in a dimensional form. Thus, to insure an accurate solution to the bow shock equation, the convergence criterion is made consistently dimensional by requiring the residual of Equation (3.12) to be less than $\varepsilon/(\Delta x)^2$, where Δx is the step size for the supersonic calculation and ε is the convergence criterion input to the code via TEST(34). This modification ensures a valid shock point solution, regardless of the length scale used in the geometric input to 3DSAP.

SECTION 4

TREATMENT OF MULTI-CONIC AFTERBODIES

In the original version of 3DSAP it was assumed that the afterbody was axisymmetric and was either a cone or a bicone. To extend the afterbody geometry capability, the modified 3DSAP allows as many as five conical segments, each of which must be axisymmetric. (The number of conical segments allowed in the new version of 3DSAP may readily be increased by increasing the dimensions of the appropriate arrays within the 3DSAP code.)

With the new version of 3DSAP the frustum geometry is always input in the same format. As shown in Figure 4.1, the $I^{\underline{th}}$ conical segment is defined by specification of RF(I), ZF(I), DZF(I), THF(I), RF(I+1), and ZF(I+1). Assuming that RF(1) and ZF(1) are known, each conical segment I is defined through specification of any one of the following pairs of parameters:

ZF(I+1), RF(I+1)
ZF(I+1), THF(I)
RF(I+1), DZF(I)
RF(I+1), THF(I)
DZF(I), THF(I).

The choice of which pair of parameters to use is left to the user, and can be varied from one conical section to the next. More specific details on the geometry definition procedure for the new version of 3DSAP are provided in Appendix A.

In addition to increasing the number of frustum geometry segments allowed, the 3DSAP code has been further modified to improve the treatment of expansion corners on the frustum. Since 3DSAP is formulated in a body-normal coordinate system, the coordinate system is discontinuous at points

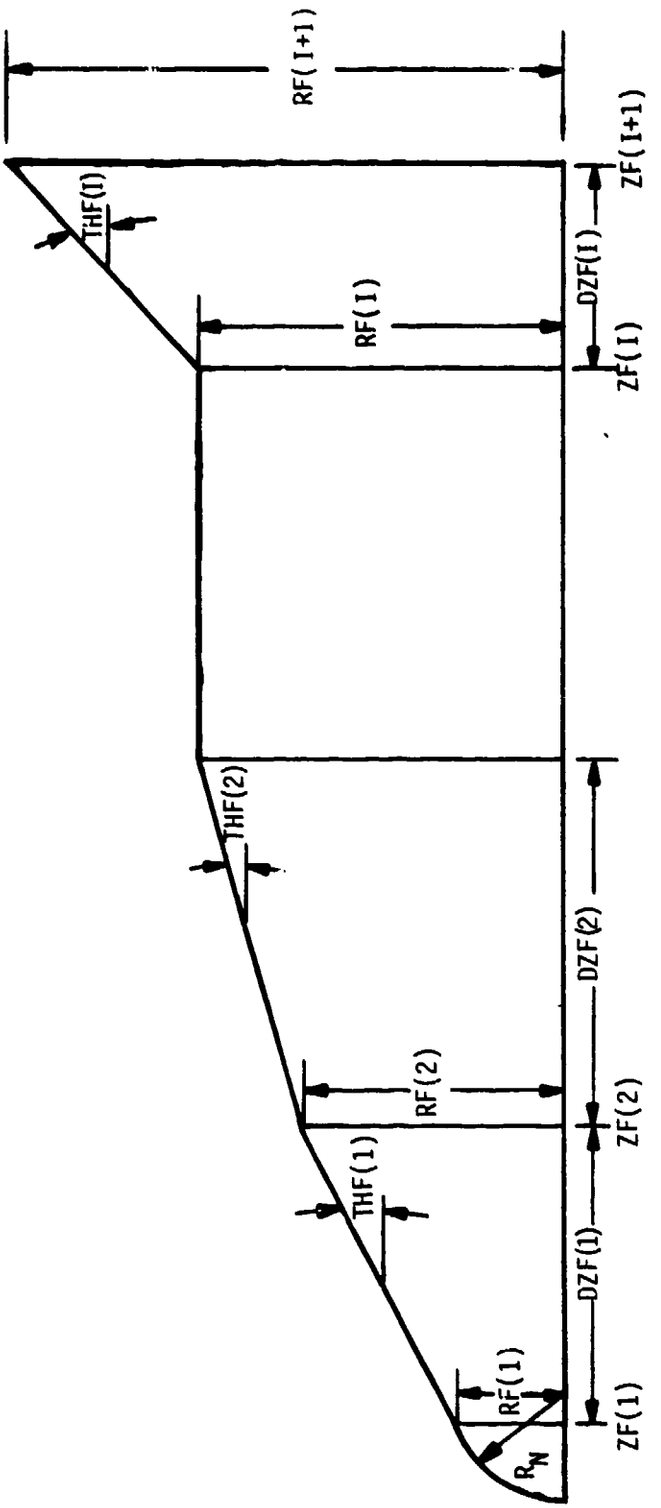

FIGURE 4.1 3DSAP FRUSTUM GEOMETRY DEFINITION

where the body slope is discontinuous. As illustrated in Figure 4.2, the discontinuous coordinate system actually fails to include a portion of the flow field at expansion corners.

To illustrate the procedure developed to treat frustum expansion discontinuities, referring to Figure 4.2, assume the flow field solution has been computed to the end of the first conic section (cone angle θ_{b_1}), with the bow shock located at $y = y_{s_1}$, and with the flow field properties P, σ, τ, s known along the body normal between the body and the shock. For the forward marching supersonic solution to be computed on the second conic section (cone angle θ_{b_2}) it is necessary to know the bow shock location $y = y_{s_2}$ measured normal to the second conic section, as well as all flow field properties along this new normal.

Because of the coordinate system discontinuity, no flow field information is available along the new body normal. However, the required information can readily be generated through the use of several approximations.

First, it is assumed that the bow shock slope as measured in a continuous (z,r) cylindrical coordinate system is constant across the body-normal coordinate system discontinuity.* Defining

$$\sigma_s = \tan^{-1} \frac{\partial r_s}{\partial z} = \theta_{b_1} + \tan^{-1} y_{s_{x_1}} \tag{4.1}$$

and assuming σ_s to be constant, it can be shown that

$$y_{s_2} = y_{s_1} \frac{\cos \theta_{b_1} + \tan \sigma_s \sin \theta_{b_1}}{\cos \theta_{b_2} + \tan \sigma_s \cos \theta_{b_2}} \tag{4.2}$$

---

*This procedure assumes that the bow shock is not highly curved in the region of the coordinate system discontinuity.

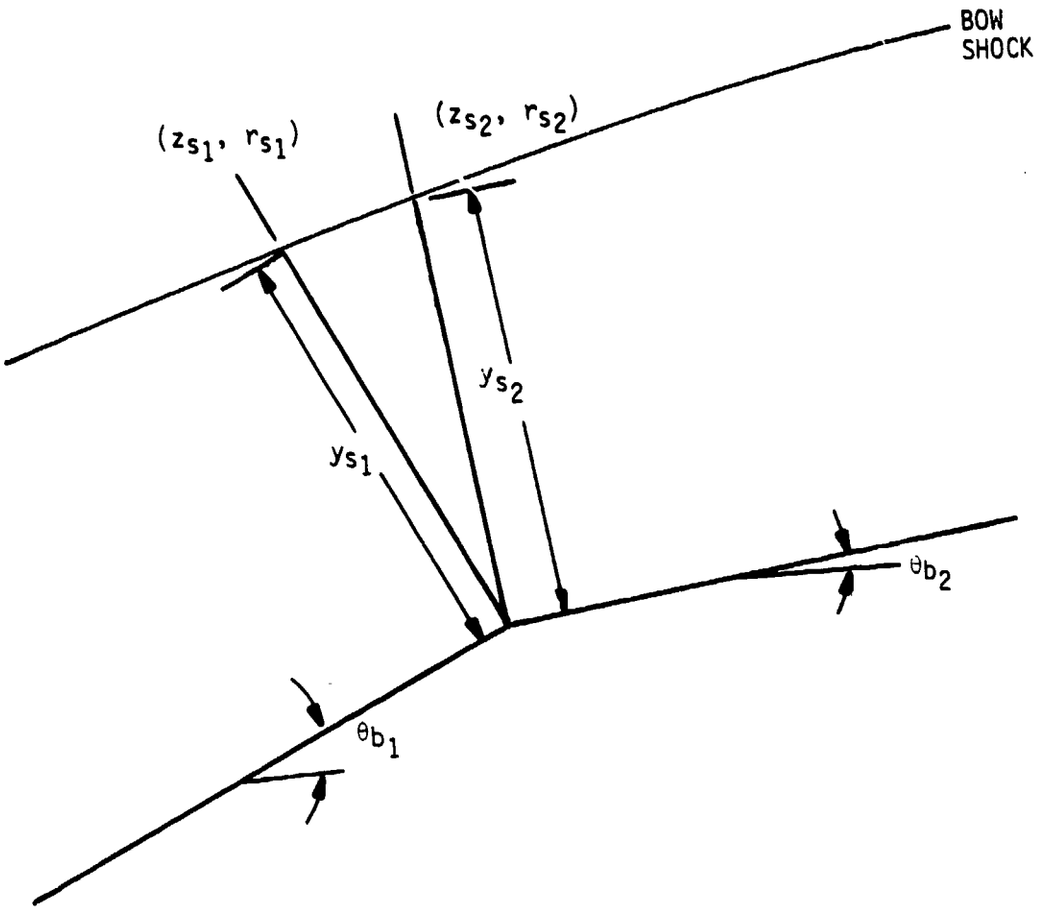

FIGURE 4.2. FRUSTUM EXPANSION CORNER

from which it follows that

$$r_{s_2} = r_b + y_{s_2} \cos \theta_{b_2} \tag{4.3}$$

$$z_{s_2} = z_b - y_{s_2} \sin \theta_{b_2} \quad . \tag{4.4}$$

The shock slope in the body-normal coordinate system relative to the second cone can then be expressed as

$$y_{s_{x_2}} = \tan (\sigma_s - \theta_{b_2}) \quad . \tag{4.5}$$

For the definition of flow field properties along the new normal, define $\eta_1 = f(y/y_{s_1})$ as the computational coordinate along the normal to the first cone, and $\eta_2 = f(y/y_{s_2})$ as the computational coordinate along the normal to the second cone. Assuming that the function f (which may involve stretching, as described in Section 3) does not vary, the pressure and entropy are assigned as

$$p(\eta_2) = p(\eta_1) \tag{4.6}$$

$$s(\eta_2) = s(\eta_1) \quad . \tag{4.7}$$

Note that, except for the body surface point, these relations would hold exactly if the first conic section were a sharp cone.

More care is required in the modification of the streamline slopes σ and τ due to the discontinuity of the body-normal coordinate system. From purely geometric considerations, it can be shown that the streamline slope σ_2 on the second cone can be expressed in terms of the slope σ_1 on the first cone, assuming a constant streamline slope in cylindrical coordinates, as

$$\sigma_2 = \frac{\sigma_1 + \tan (\theta_{b_1} - \theta_{b_2})}{1 - \sigma_1 \tan (\theta_{b_1} - \theta_{b_2})} \quad . \tag{4.8}$$

To recompute the circumferential streamline slope τ it is first assumed that the total velocity, defined as

$$q = \sqrt{u_1^2(1 + \sigma_1^2 + \tau_1^2)} = \sqrt{u_2^2\ (1 + \sigma_2^2 + \tau_2^2)} \tag{4.9}$$

can be determined from

$$q(n_2) = q(n_1) \quad . \tag{4.10}$$

Since the cross-flow velocity component w is not affected by the body-normal system discontinuity, it follows that

$$\tau_2 = \frac{w_2}{u_2} = \frac{w_1}{u_2} = \frac{w_1}{u_1}\ \frac{u_1}{u_2} \quad . \tag{4.11}$$

Combining (4.9) and (4.11) yields

$$u_2 = \sqrt{\frac{q^2 - \tau_1^2\ u_1^2}{1 + \sigma_2^2}} \tag{4.12}$$

and finally

$$\tau_2 = \tau_1 \frac{u_1}{u_2} \quad . \tag{4.13}$$

The procedure described above is used to generate the necessary data along the normal to the second cone for all grid points, except for the body point. At the body point at the discontinuity, the pressure on the second cone is redefined from the series expansion of the Prandtl-Meyer relation for an ideal gas:

$$\frac{p_2}{p_1} = 1 - \frac{\gamma M_1^2}{\sqrt{M_1^2-1}}\ (\Delta\theta) + \gamma M_1^2\ \frac{(\gamma+1)M_1^4 - 4\ (M_1^2 - 1)}{4(M_1^2 - 1)^2}\ (\Delta\theta)^2 \tag{4.14}$$

where $\Delta\theta = \theta_{b_1} - \theta_{b_2}$. This expansion is also used for real gas calculations to approximate the pressure drop across the expansion corner, using the upstream value of γ.

At this body point (on the second cone) the kinematic boundary condition requires the $\sigma_2 = 0$, and the isentropic expansion process requires $s_2 = s_1$. The new u velocity component can then be computed from the conservation of total enthalpy for an inviscid flow:

$$u_2 = \sqrt{2\,(H_\infty - h_2) - u_1^2\,\tau_1^2} \tag{4.15}$$

where $h_2 = h_2\,(p_2, s_2)$. Finally, the circumferential streamline slope at the body can be redefined from Equation (4.13).

SECTION 5

CALCULATION OF FLARED AFTERBODIES

The major development effort in the modification of the 3DSAP code has been the addition of the capability to treat flared afterbody sections. The calculation procedure for flared afterbody sections described in this section was developed subject to the following assumptions:

- the frustum has only one flare (i.e., compression corner);
- the flare section must be the last frustum conic section;
- the flare section flow field must have an embedded shock of finite strength that is attached at all points of the compression discontinuity; and
- the flow behind the embedded shock must remain sufficiently supersonic so that the finite-difference forward marching integration procedure for supersonic flows remains valid.

With these assumptions, a discrete shock-fitting approach was selected as the solution procedure for the flared afterbody flow field. In this approach the flare shock layer is divided into two regions, one between the body and the embedded shock and the other between the embedded shock and the bow shock. The embedded shock, which serves as the boundary between the two regions, is explicitly treated as a discontinuity across which the Rankine-Hugoniot shock jump conditions are enforced.

An alternate approach to the calculation of the flare flow field is the use of the "conservation" form of the governing equations, which has the capability of automatically "capturing" the embedded shock without requiring any special procedures to calculate the position and strength of the embedded shock. However, the use of this "shock-capturing" technique

will produce oscillations in the flow field in the vicinity of the embedded shock; these oscillations can be large enough to cause the solution to fail. "Conservation" form solutions frequently use numerical damping to control these oscillations and thus obtain a solution, but if too much damping is used, the calculated inviscid flow field can be distorted.

Because of this consideration, and the desire to have an algorithm that will work with minimal intervention required of the user, the shock-fitting approach was selected for this effort even though the development of a shock-fitting procedure requires greater analytical effort than does the development of a "shock-capturing" scheme.

The shock-fitting computational scheme has been incorporated into a new subroutine, FLARE, which is called from the subroutine SHPR when a compressive geometric discontinuity is encountered in the frustum flow field calculation. (Thus, when using 3DSAP on configurations that do not have flares, some core storage can be saved by not loading the subroutine FLARE.)

The first step in the flared body calculation is the initialization of the embedded shock at the compression corner. In each meridional plane being computed, it is necessary to determine the slope of the embedded shock such that the downstream flow is tangent to the body surface. Following the procedure outlined in Section 4 for expansion corners, the computed flow field solution on the conic section upstream of the flare is rotated to the body-normal coordinate system for the flare section, but without modifying the surface pressure or imposing the kinematic boundary condition at the body point. Let these data at the body be denoted by p_1, σ_1, τ_1, and s_1, noting that $\sigma_1 < 0$.

The embedded shock initialization problem for an axisymmetric frustum reduces to finding the slope of the embedded shock such that the properties downstream of the shock (denoted by p_2, σ_2, τ_2, and s_2) satisfy the flow tangency condition, $\sigma_2 = 0$.

To allow for real gas solutions, an iterative process is used to determine the initial embedded shock slope in each meridional plane being computed. If the unit normal to the embedded shock is denoted by

$$\hat{N} = N_1 \hat{e}_x + N_2 \hat{e}_y \tag{5.1}$$

as shown in Figure 5.1, the upstream velocity normal to the shock is

$$\tilde{u}_1 = -u_1 N_1 - u_1 \sigma_1 N_2 \quad . \tag{5.2}$$

Knowing $\tilde{u}_1$, p_1, and s_1, the downstream properties $\tilde{u}_2$, p_2, and s_2 can be determined from the Rankine-Hugoniot conditions from a call to the 3DSAP subroutine SHOCK for both ideal and real gases.

The velocities downstream of the embedded shock can be determined from the relations

$$u_2 = u_1 - N_1 (\tilde{u}_1 - \tilde{u}_2) \tag{5.3}$$

$$u_2 \sigma_2 = u_1 \sigma_1 - N_2 (\tilde{u}_1 - \tilde{u}_2) \quad . \tag{5.4}$$

In the iteration, the value of N_2 is varied with

$$N_1 = -\sqrt{1 - N_2^2} \quad , \tag{5.5}$$

until, from Equation (5.4), the tangency condition $\sigma_2 = 0$ is satisified. With the embedded shock surface defined as $y = y_{s_2}(x,\phi)$, the appropriate embedded shock slope becomes

$$y_{s_{2_x}} = -N_1/N_2 \quad . \tag{5.6}$$

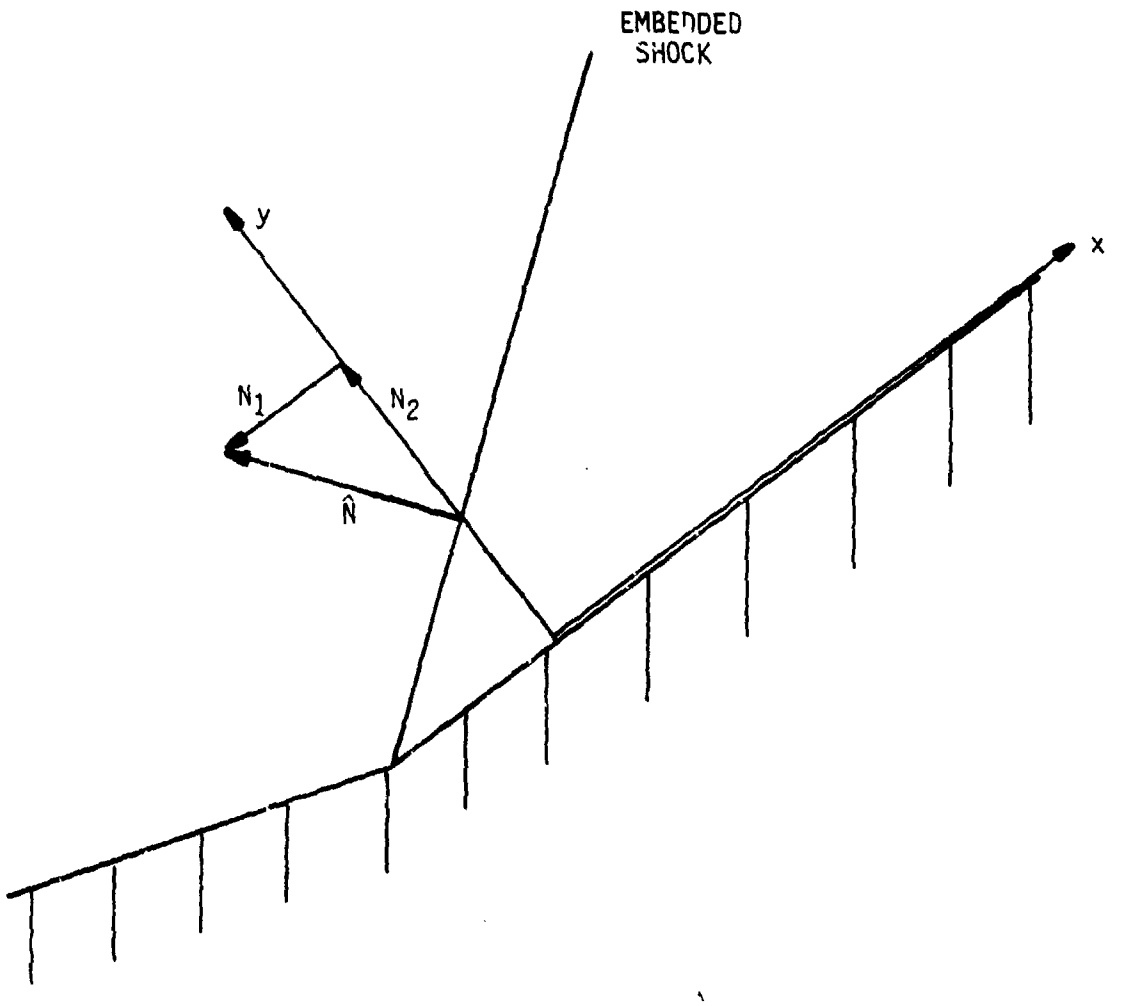

FIGURE 5.1. EMBEDDED SHOCK INITIALIZATION

The initialization for the two layer flare flow field calculation is carried out as shown in Figure 5.2. With the bow shock surface denoted by $y = y_{s_1}(x,\phi)$, Region I is defined as $y_{s_2} < y < y_{s_1}$, and Region II as $0 < y < y_{s_2}$. Computational transformations of the normal coordinate are carried out separately in each region (and may include stretching), resulting in

$$\eta_1 = f_1\left(\frac{y - y_{s_2}}{y_{s_1} - y_{s_2}}\right) \tag{5.7}$$

$$\eta_2 = f_2\left(\frac{y}{y_{s_2}}\right) \tag{5.8}$$

where the form of the functions f_1 and f_2 is that given in Section 3 when stretching is used.

The initial data surface is established at a small but finite distance Δx from the compression corner in each meridional plane as shown in Figure 5.2, where the bow and embedded shock positions are given by

$$y_{s_1} = y_{s_{1_o}} + y_{s_{1_x}}(\Delta x) \tag{5.9}$$

$$y_{s_2} = y_{s_{2_x}}(\Delta x) \tag{5.10}$$

The field data in Region I is assigned directly from the solution upstream of the flare, rotated into the body-normal coordinate system of the flare section. This region will initially have the same number of grid points in the normal direction as did the upstream solution. Region II, because of its small size, is initialized with two grid points, one at the body and one at the embedded shock, and both points have the properties downstream of the embedded shock assigned.

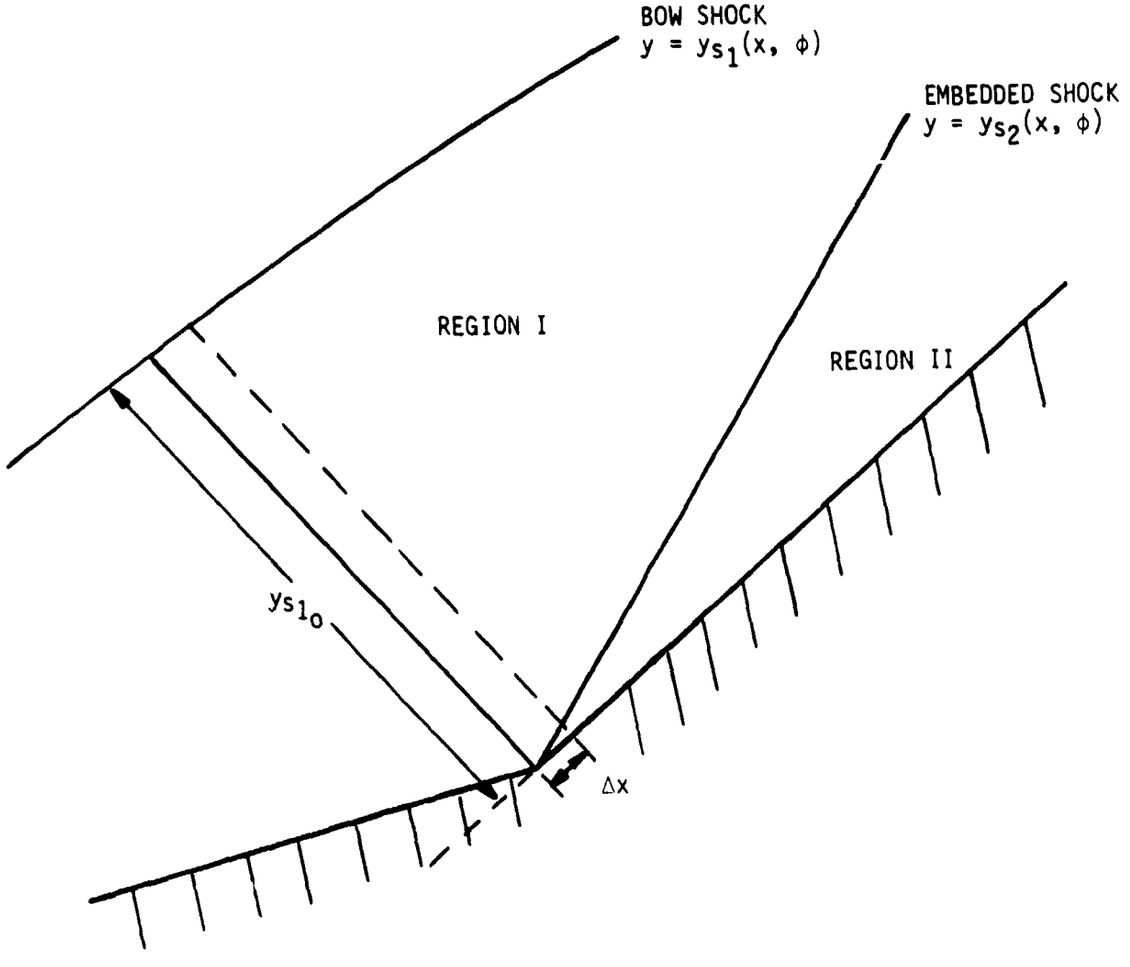

FIGURE 5.2. FLARE CALCULATION INITIALIZATION

The computational procedure used in this flared body subroutine is exactly that used in the subroutine SHPR, with the following exceptions:

1.) The "body" point in Region I (which is the upstream point at the embedded shock) is treated as a field point, using one-sided forward differences to approximate η-derivatives.

2.) Shock point calculations (at both the bow and embedded shocks) are performed using the non-iterative Kentzer-Moretti predictor-corrector[8,9] algorithm.

In the Kentzer-Moretti approach to shock-point calculations, differentiated forms of the Rankine-Hugoniot conditions are incorporated into the appropriate characteristic compatibility condition to yield an equation for shock curvature, which can be integrated twice to obtain shock slope and position.

The form of the compatibility condition used is exactly that given by Equation (3.12), with the additional simplification of $H = 1$ allowed by consideration of only conic sections on the afterbody.

For both the bow and embedded shocks, let $(\ )_1$ denote properties upstream of the shock and $(\ )_2$ denote downstream properties. It is then possible to differentiate the Rankine-Hugoniot conditions to obtain

$$P_{2\xi} = D_1 P_{1\xi} + D_2 \tilde{u}_{1\xi} + D_3 s_{1\xi} \tag{5.11}$$

$$\tilde{u}_{2\xi} = D_4 P_{1\xi} + D_5 \tilde{u}_{1\xi} + D_6 s_{1\xi} \quad , \tag{5.12}$$

where $\tilde{u}_1 = -u_1 (N_1 + \sigma_1 N_2 + \tau_1 N_3)$

$N_1 = -y_{s_x}/\nu$

$N_2 = 1/\nu$

$N_3 = -y_{s_\phi}/r_s\nu$

$\nu = \sqrt{1 + y_{s_x}^2 + y_{s_\phi}^2/r_s^2}$.

It can be noted that for the bow shock, where $P_1 = \ell n\ p_\infty$ and $s_1 = s_\infty$, that $P_{1_\xi} = s_{1_\xi} = 0$. For an ideal gas, the coefficients D_i may be expressed in relatively simple form as

$$D_1 = \frac{2\tilde{u}_1^2 - (\gamma-1)\ a_1^2}{2\gamma\tilde{u}_1^2 - (\gamma-1)\ a_1^2}$$

$$D_2 = \frac{1}{\tilde{u}_1}\ \frac{4\gamma\tilde{u}_1^2}{2\gamma\tilde{u}_1^2 - (\gamma-1)\ a_1^2}$$

$$D_3 = \frac{-2\tilde{u}_1^2\ (\gamma-1)}{2\gamma\tilde{u}_1^2 - (\gamma-1)\ a_1^2}$$

$$D_4 = \frac{2\ (\gamma-1)\ a_1^2}{\gamma\ (\gamma+1)\ \tilde{u}_1}$$

$$D_5 = \frac{1}{\gamma+1}\ (\gamma-1 - \frac{2a_1^2}{\tilde{u}_1^2}\ )$$

$$D_6 = D_4$$

For a real gas (equilibrium), the forms of the D_i coefficients are more complicated and are not presented here.

Other terms necessary for this shock point equation are as follows:

$$N_{1\xi} = C_1\, y_{s_{xx}} + C_2 \tag{5.13}$$

$$N_{2\xi} = C_3\, y_{s_{xx}} + C_4 \tag{5.14}$$

$$N_{3\xi} = C_5\, y_{s_{xx}} + C_6 \tag{5.15}$$

$$\tilde{u}_{1\xi} = C_7\, y_{s_{xx}} + C_8 \tag{5.16}$$

$$u_{2\xi} = C_9\, y_{s_{xx}} + C_{10} \tag{5.17}$$

$$v_{2\xi} = C_{11}\, y_{s_{xx}} + C_{12} \tag{5.18}$$

with the coefficients C_i given by

$$C_3 = N_2^2 N_1$$

$$C_4 = N_2^2 N_3 \left(y_{s_{x_\phi}}/r_s - y_{s_\phi}\, y_{s_x}/r_s^2\right)$$

$$C_1 = -C_3\, y_{s_x} - N_2$$

$$C_2 = -y_{s_x}\, C_4$$

$$C_5 = -y_{s_\phi}\, C_3/r_s$$

$$C_6 = -y_{s_\phi}\, C_4/r_s - N_2 \left(y_{s_{x_\phi}}/r_s - y_{s_\phi}\, r_{s_x}/r_s^2\right)$$

$$C_7 = -u_1 \, (C_1 + \sigma_1 \, C_3 + \tau_1 \, C_5)$$

$$C_8 = -u_{1\xi} \, (N_1 + \sigma_1 \, N_2 + \tau_1 \, N_3) - u_1 \, (N_2 \, \sigma_{1\xi} + N_3 \, \tau_{1\xi})$$
$$-u_1 \, (C_2 + \sigma_1 \, C_4 + \tau_1 \, C_6)$$

$$C_9 = -(\tilde{u}_2 - \tilde{u}_1) \, C_1 - N_1 \, (D_5 - 1) \, C_7$$

$$C_{10} = u_{1\xi} - N_1 \, (D_4 \, P_{1\xi} + D_6 \, s_{1\xi}) - N_1 \, (D_5 - 1) \, C_8$$
$$-(\tilde{u}_2 - \tilde{u}_1) \, C_2$$

$$C_{11} = -N_2 \, (D_5 - 1) \, C_7 - (\tilde{u}_2 - \tilde{u}_1) \, C_3$$

$$C_{12} = \sigma_1 \, u_{1\xi} + u_1 \, \sigma_{1\xi} - N_2 \, [D_4 \, P_{1\xi} + D_6 \, s_{1\xi} + C_8 \, (D_5 - 1)]$$
$$-(\tilde{u}_2 - \tilde{u}_1) \, C_4 \quad .$$

With substitution of the above expressions into the characteristic compatibility condition, solving for the shock curvature yields

$$y s_{xx} = [-\frac{af_y}{u} \beta_1 \, (D_1 \, P_{1\xi} + D_3 \, s_{1\xi}) + \frac{\gamma}{u} \, (A - f_x) \, C_{10}$$
$$- \frac{\gamma}{u} \, f_y \, C_{12} + (RHS)] / [\frac{af_y}{u} \beta_1 \, D_2 \, C_7 \qquad (5.19)$$
$$- \frac{\gamma}{u} \, (A - f_x) \, C_9 + \frac{\gamma}{u} \, f_y \, C_{11}]$$

where unsubscripted quantities are evaluated with properties downstream of either the bow or embedded shock, as appropriate.

Integrating this equation twice yields both the shock slope (y_{s_x}) and the shock position (y_s). Knowing the shock slope, the properties downstream of the shock can be determined directly using the SHOCK subroutine.

As part of the flared afterbody calculation procedure, logic has been included to automatically respace Regions I and II to ensure that sufficient field points are used to describe the region between the body and the embedded shock as the shock moves away from the body, and to ensure that the mesh spacing between the embedded and bow shocks does not get too small. The respacing criteria built into the code thus ensure adequate resolution, without unnecessarily small step sizes (which will adversely affect the efficiency of the calculation).

A procedure has also been developed to treat, in an approximate manner, the intersection of the embedded and bow shocks. The two shocks are assumed to intersect when, in any meridional plane, the shocks come within some arbitrary percentage of the total shock layer thickness of each other (typically 5%). When this occurs in any one plane, the shocks are assumed to intersect in all planes at points determined by extending the bow and embedded shocks with constant slopes (y_{s_x}) assumed. At the assumed points of intersection, the exact solutions for properties downstream of intersecting shocks of the same family are obtained (including the slope of the resultant shock). The slopes of the resultant shocks are then extrapolated back to the last station computed, a new "resultant shock layer thickness" is defined, and the one region afterbody solution is continued using the subroutine SHPR.

It should be noted that in many, if not most, of the flared configurations of interest that the bow and embedded shocks typically intersect downstream of the aft end of the vehicle.

SECTION 6

REFERENCES

1. Hall, D. W., "The Three-Dimensional Shock and Pressure (3DSAP) Approximate Flow Field Technique, Vol. I. Engineering Analysis," SAMSO TR-77-C145, May 1977.

2. Dougherty, C. M. and Hall, D. W., "The Three-Dimensional Shock and Pressure (3DSAP) Approximate Flow Field Tecnnique, Vol. II. User's Manual," SAMSO TR-77-C145, May 1977.

3. Taylor, S., Siemons, E., Kyriss, C., and Hall, D., "Performance Technology Program (PTP-S II), Vol. VII.; Low Altitude Roll/Trim Dispersion Modeling for Ballistic Reentry Vehicles," BMO-TR- (to be published).

4. Kyriss, C. L. and Neff, R. S., "An Approximate Flow Field Technique for Ablated Re-entry Configurations (NOSAR)," General Electric TIS 73SD201, January 1973.

5. Love, E. S., Woods, W. C., Rainey, R. W., and Ashby, G. C., Jr., "Some Topics in Hypersonic Body Shaping," AIAA Paper 69-181, January 1969.

6. Abbett, M. J. and Davis, J. E., "Passive Nosetip Technology (PANT) Program, Volume IV. Heat Transfer and Pressure Distribution on Ablated Shapes, Part II. Data Correlation and Analysis," SAMSO TR-74-86, Vol. IV, Part II, January 1974.

7. Moretti, G., "Calculation of the Three-Dimensional, Supersonic, Inviscid, Steady Flow Past an Arrow-Winged Airframe," Polytechnic Institute of New York, POLY-AE/AM Report No. 76-8, May 1976.

8. Kentzer, C. P., "Discretization of Boundary Conditions on Moving Discontinuities," Second International Conference on Numerical Methods in Fluid Dynamics, University of California, Berkeley, Calif., September 1970.

9. Moretti, G. and Pandolfi, M., "Entropy Layers," Polytechnic Institute of Brooklyn, New York, PIBAL Report No. 71-33, 1971.

APPENDIX A. USER'S GUIDE TO 3DSAP

This Appendix describes the input variables required for the operation of the updated 3DSAP code. These input variables are discussed in groupings of geometry specification, freestream conditions, output controls, and special options. A glossary of all input variables is provided in Appendix B.

A. GEOMETRY

The geometry specifications required in 3DSAP are described below. Nosetip geometries may be arbitrary, or one of several analytic options. The frustum geometry inputs allow for the definition of axisymmetric multi-conic configurations.

1. NOSE GEOMETRY

Arbitrary

Arbitrary nose geometries are specified by defining cross-sections perpendicular to the vehicle centerline, as shown in Figure 1. Cross-sections are defined in terms of the polar coordinates RBD(K,M) and PHIBD(M) at the axial stations ZBD(K), relative to the center of each cross-section. defined from the arrays D1(K) and D2(K). Note that the cross-section centers need not lie along the vehicle axis.

Options are provided for specification of special types of cross-sections, as discussed in Reference 2. The option exercised is determined by the number of meridional planes of geometry input, and the appropriate values of PHIBD are generated automatically as follows:

No. of Planes Input	Geometry	PHIBD
1	circular	0
2	elliptic	0,$\pi/2$
3	bi-elliptic	0,$\pi/2$,π
4(ISA = 2 only*)	quad-elliptic	0,$\pi/2$, π, $3\pi/2$

If more than four planes of gemoetry are input (three planes, for ISA = 1) the cross-sections are taken to be arbitrary and the PHIBD array must be specified.

The surfaces to be computed in the nose calculation, defined as $\hat{\phi}$ = constant, are specified by the user with the PHI(M) array. Appropriate radii at each cross-section for each $\hat{\phi}$ value are determined analytically for the special cross-section options listed above; for the case of general cross-sections the radii are determined by cubic spline interpolation.

If the user does not specify the number of surfaces to be computed, the PHI array is automatically set to provide for surfaces spaced 90^0 apart; for a pitch plane of geometric symmetry without sideslip (ISA = 1), the surfaces to be computed are $\hat{\phi}$ = 0, $\pi/2$, and π. Without a plane of symmetry (ISA = 2), the surfaces are $\hat{\phi}$ = 0, $\pi/2$, π and $3\pi/2$. ($\hat{\phi}$ is defined such that $\hat{\phi}$ = 0 corresponds to the lee plane for positive angle of attack, and $\hat{\phi}$ = π to the wind plane.)

For geometries with a pitch plane of symmetry that have general cross-sections and are to be run at sideslip (requiring ISA = 2), it is possible to define only the half-planes of the arbitrary cross-sections, imposing symmetry of the geometry about the pitch plane by specifying the $\hat{\phi}$ = π plane as MSYM.

---

*ISA is a flag, set to one if a pitch plane of gemoetric symmetry exists and the sideslip is zero; otherwise, ISA is set to two.

The stagnation point on arbitrary nose geometries in 3DSAP is defined by the user-supplied values of D1(1) and D2(1); RBD(1) must always be zero. This point will be common to all surfaces PHIBD(M) and PHI(M). In addition, the last point of the nose geometry, which must coincide with the start of the frustum, must have D1 and D2 both zero, and all values of RBD at this station must be equal to RF(1) (see frustum geometry definition).

Analtyic

Options exist within the 3DSAP for the analytic definition of spherical, elliptic, and biconic nosetips. A spherical nosetip, with radius RN, is assumed if no ZBD's are input, and IBIC = 0 and IELL = 0. The axial location of the geometric stagnation point is assigned to be Z = DELZ.

If IELL $\neq$ 0, an elliptic nosetip is assumed, with the ratio of major to minor axes defined as AB(a/b), as shown in Figure A.1. Setting IBIC $\neq$ 0 allows a biconic nosetip to be defined by the parameters THN, RC, and RN, as shown in Figure A.1. Note that Z = 0 is defined as the virtual apex location of the first conical afterbody segment for both the elliptic and biconic nosetip analytic geometry options.

2. FRUSTUM GEOMETRY

The definition of the frustum geometry in this modified version of 3DSAP requires the specification of values for the arrays ZF, RF, DZF, and THF (see Figure 4.1). The frustum is assumed to be an axisymmetric multi-conic, with NCON conic sections (maximum of 5). Values for RF(1) and ZF(1) must always be provided (except for a spherical nosetip), and each conical segment I is defined through specification of any of the following pairs of parameters:

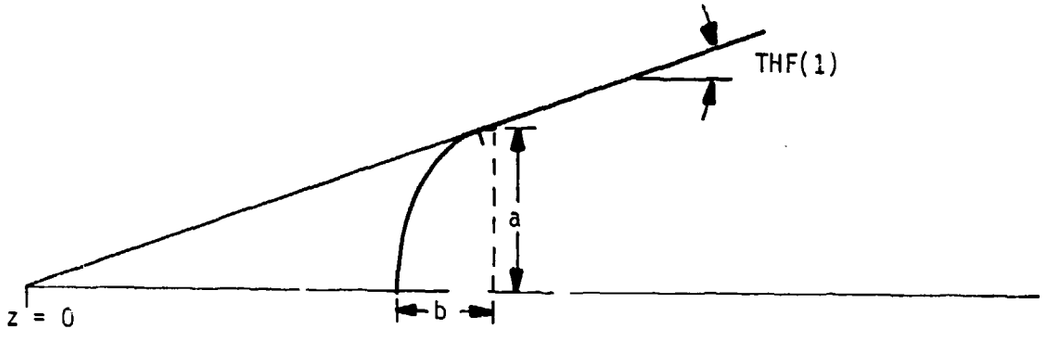

a.) ELLIPTIC NOSETIP

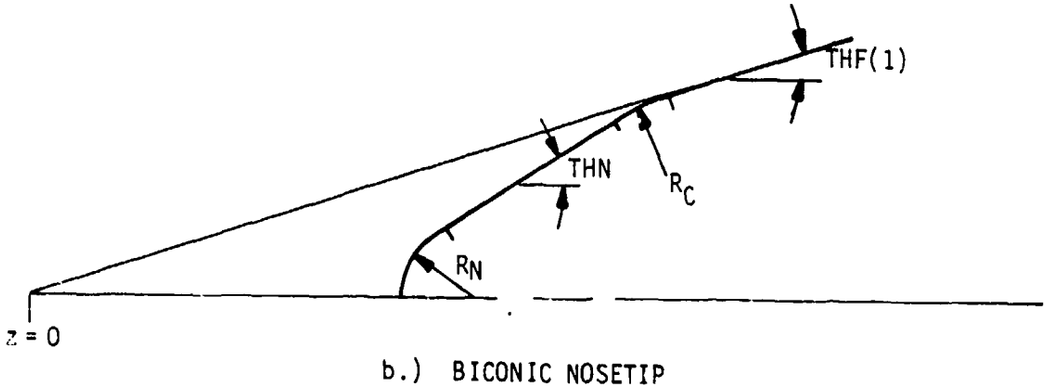

b.) BICONIC NOSETIP

FIGURE A.1. ANALYTIC DEFINITION OF ELLIPTIC AND BICONIC NOSETIPS

ZF(I+1), RF(I+1)
ZF(I+1), THF(I)
RF(I+1), DZF(I)
RF(I+1), THF(I)
DZF(I), THF(I)

Cylindrical segments (THF(I) = 0.) cannot be defined using the RF(I+1), THF(I) pair.

B. FREESTREAM PROPERTIES

For each calculation it is necessary to specify the freestream Mach number (AMINF) or the freestream velocity (QINF), as well as the static pressure and temperature (PINF and TINF). Values of PINF and TINF will be generated automatically from the 1962 standard atmosphere tables by specifying the desired altitude (ALT) and the flat IATMP = 62 for the 1962 U.S. Standard tables or IATMP = 59 for the 1959 ARDC tables. For non-dimensional ideal gas calculations, PNIF and TINF are set to 1.0 (default values). Care must be exercised when specifying QINF for non-dimensional ideal gas calculations, since then QINF = $V_\infty/\sqrt{p_\infty/\rho_\infty}$, as discussed below.

The orientation of the vehicle relative to the freestream velocity vector is defined by specification of the angle of attack (ALPHA) and the sideslip angle (BETA). Note that positive angle of attack implies nose up, and positive sideslip angle implies nose left.

Units

IDEAL GAS (IRG = 0)

The standard operating procedure for ideal gas calculations is to use non-dimensional variables, in which PINF = TINF = RIDEAL = 1. With this normalization the variables in 3DSAP take the forms:

3DSAP	ACTUAL
p	p/p_∞
ρ	ρ/ρ_∞
T	T/T_∞
(u,v,w)	$(u,v,w)/\sqrt{p_\infty/\rho_\infty}$.

Note that with this formulation the gas law becomes $p = \rho T$. The isentropic exponent is specified as GIDEAL. If desired, a compressibility factor (ZIDEAL) may also be specified.

Dimensional ideal gas calculations are also possible, requiring only that a dimensionally consistent value of RIDEAL is specified, as well as appropriate values of PINF and TINF.

REAL GAS (IRG = 1)

All quantities in real gas calculations are dimensional with the units:

p	lbf/ft^2
ρ	$slugs/ft^3$
T	^oR
(u,v,w)	ft/sec .

The real gas thermodynamic properties used in 3DSAP are for equilibrium air. The gas properties required during the calculation are obtained by interpolation on the thermodynamic property tables supplied with the code.

C. OUTPUT CONTROLS

This section details the input variables that control the type of output generated by the 3DSAP code.

1. STANDARD FORMAT

The standard output of 3DSAP consists of the following:

a.) surface pressure and shock shape for each surface on the nose,

b.) summary of force and moment data on the nose at each axial station specified,

c.) surface pressure and shock shape for each plane on the frustum,

d.) summary of force and moment data on the frustum at each axial station computed.

Force and moment coefficients are normalized using a local reference area (πr^2) ard the local reference length (z, measured from the arbitrary point z = 0). Options are available to the user to specify a reference area (AREF) and a reference length (ALREF) to be used at all stations. In addition, an arbitrary moment reference point may be used by specifying XBAR, YBAR, and/or ZBAR.

2. OPTIONAL OUTPUT

Additional output which may be generated includes:

a.) tables of shock properties (KENSE(1) $\neq$ 0),

b.) field data (data printed every IPRINT stations beginning with station MPRINT).

D. SPECIAL PROVISIONS AND OTHER CONTROLS

3DSAP has input parameters and options other than those described above, designed to provide the user with a high degree of flexibility in the application of the code. These parameters and options are described below.

Global Transonic Iteration

As discussed in References 1 and 2, 3DSAP has the option of performing a global iteration on shock slopes in the approximate transonic solution on the nose. Although not normally exercised in the standard operating procedure of 3DSAP, this global iteration can be implemented by setting ISHK to zero. The use of this global iteration is discussed in Reference 2.

Surface Entropy Relaxation

In the standard operating procedure of 3DSAP the surface entropy is assigned the stagnation value, since the stagnation streamline wets the body surface in inviscid flow. However, as the length of the frustum approaches infinity, the vortical layer induced by a blunt nosetip becomes singular. (Such a situation would be encountered if a sharp cone solution were sought as the limit of a blunted cone solution as the bluntness ratio goes to zero.) To avoid this problem, the surface entropy in the windward plane of the frustum may be relaxed by determining its value by extrapolation of the entropies at the two adjacent field points on the body normal. This option is exercised by setting ICS equal to zero.

Termination of the Calculation

In normal usage, 3DSAP terminates when the end of the frustum has been reached in the forward-marching computational procedure. For code check-out purposes, it is sometimes convenient to compute only a predetermined

number of steps on the frustum. 3DSAP can be terminated before the end of the frustum is reached by specifying the number of computational steps to be taken on the frustum, MTERM.

Intervals Across the Shock Layer

Since it is a complete flow field technique, 3DSAP determines properties across the shock layer (along body normals) as well as surface pressures and shock shape. Two input parameters are available in 3DSAP to control the point spacing between the body and the shock along body normals, NMAX1 and NMAX2. NMAX1 is the number of points used across the shock layer in the transonic solution and is usually set to five. Points in the transonic region are equally spaced in stream function across the body normal (vonMises coordinates). For supersonic calculations, both on the nose and the frustum, the number of points used is determined by NMAX2. Points in the supersonic calculation are equally spaced in distance from the body, measured along the body normal. The standard value of NMAX2 is ten, although other values may be appropriate depending on the freestream Mach number, as discussed in Section 6.

Definition of Transonic Region

3DSAP automatically determines the end point of the transonic region in each nose surface being computed by taking the more downstream of:

a.) the body point that is NSON input points downstream of the sonic point (which is determined from a correlation based on local body slope), or
b.) the most forward point such that no downstream point has a surface slope relative to the freestream velocity vector of greater than 45^{o}.

For most applications, a value of NSON equal to one will provide an adequate definition of the transonic regions. By careful choice of NSON, however, the user has the ability to enlarge the transonic region, if so desired.

Nosetip Pressure Correlation Option

As described in Section 2 of this report, a new nosetip pressure correlation which was developed for indented nosetip geometries has been added as an option to 3DSAP. This new correlation will automatically be used for arbitrary nosetip geometries, or if the user sets IPRESS = 2. The original correlation described in Reference 1 will automatically be used for analytic nosetip geometries, or if the user sets IPRESS = 1.

Normal Coordinate Stretching

The stretching of the normal coordinate to concentrate mesh points near the vehicle surface, as described in section 3, is invoked by specifying a value for the stretching parameter, α^*(ALPHSTR). The effect of this stretching parameter is illustrated in Figure 3.1. Different values of α^* may be assigned to the bow and embedded shocks by specifying ALPHSTR(1) and ALPHSTR(2), respectively.

Pressure Profile Exponent

The assumed pressure profile across the shock layer in the transonic solution of 3DSAP takes the form

$$p(\psi) = p_b + (\frac{\psi}{\psi_s})^{ANEXP}(p_s - p_b)$$

where ANEXP = 2 in the original version of 3DSAP (Reference 1). In the current version of 3DSAP, ANEXP has been pre-set to 0.75 (recommended value), but the user can modify this value by specifying a different value for ANEXP.

APPENDIX B. GLOSSARY OF INPUT VARIABLES

(Default values shown in parentheses at right)

AB	Ratio of major to minor axes for elliptic nosetip (analytic elliptic nosetip geometry option)	
ALPHA	α, Angle of attack (degrees)	
ALPHSTR(I)	α^*, Stretching parameters for normal grid stretching; I = 1 for Region I and I = 2 for Region II (for flared bodies) of frustum calculation	(0.)
ALREF	Reference length for moment coefficients (if zero, local z used)	
ALT	Altitude (feet), if IATMP used	
AMINF	M_∞, Freestream Mach number (if QINF not input)	
ANEXP	Exponent for assumed pressure profile across the nosetip shock layer (transonic region)	(0.75)
AREF	Reference area for force and moment coefficients (if zero, local πr_b^2 used)	
BETA	β, Sideslip angle (degrees)	
DELZ	Axial location of the geometric stagnation point for a spherical nosetip	(0.0)
DZF(I)	Array of axial lengths of conical frustum segments (NCON values)	
D1(K)	d_1, Vertical offset of nose cross-section center, maximum value of K = 25	
D2(K)	d_2, Lateral offset of nose cross-section center, maximum value of K = 25	
GIDEAL	γ, Ideal gas isentropic exponent	(1.4)
IATMP	Atmospheric freestream property assignment indicator: = 62 Freestream pressure and temperature from 1962 standard atmosphere = 59 Freestream pressure and temperature from 1959 ARDC tables	(0)

IBIC	≠ 0 For analytic biconic nosetip geometry option	
ICS	Surface entropy relaxation indicator: = 0 Surface entropy relaxed in wind plane = 1 No entropy relaxation	(1)
IELL	≠ 0 For analytic elliptic nosetip geometry option	
IPRESS	Nosetip pressure correlation option flag = 1 For spherical nosetip correlation = 2 For indented nosetip correlation	
IPRINT	Print increment control for field output	(1)
IRG	Real gas option indicator: = 0 For ideal gas thermodynamics = 1 For equilibrium air thermodynamics	
ISA	Plane of symmetry indicator: = 1 Pitch plane of symmetry and $\beta = 0$ = 2 Asymmetric shape or $\beta \neq 0$	(1)
ISHK	Global transonic iteration indicator: = 0 For global iteration on transonic shock slopes = 1 For assignment of transonic shock slopes	(1)
KENSE(1)	Shock table output indicator: > 0 Shock tables printed out as part of calculation < 0 Code generates shock tables only	(0)
KMAX	Number of points per meridional plane on nose - maximum of 25 (required for analytically defined spherical nose only)	(15)
MPRINT	Station at which printing of field output begins	(999)
MSYM	Index of meridional surface about which the geometry is symmetric	
MTERM	Number of steps to be taken (if termination desired before z = ZF(NCON + 1))	(999)
NCON	Number of conical segments on the frustum (maximum of 5)	(1)
NITER	Maximum number of global transonic iterations, if ISHK = 0	(100)

NMAX1	Points between body and shock - transonic (maximum of 20)	(5)
NMAX2	Points between body and shock - supersonic (maximum of 20)	(10)
NSON	Number of points beyond sonic point to be included in transonic region	(0)
NUWTB	Number of entries in shock table	(91)
PHI(M)	ϕ, Meridional angles of surfaces to be calculated on nose (deg.) (maximum value of M = 8)	(ISA = 1 0^o,90^o.180^o) (ISA = 2 0^o,90^o,180^o,270^o)
PHIBD(M)	$\hat{\phi}$, Meridional angles of surfaces in which arbitrary nose geometry is defined (Deg.) (maximum value of M = 8)	
PINF	p_∞, Freestream static pressure (Real Gas, lbf/ft^2)	(1.0)
QINF	q_∞, Freestream velocity (if AMINF not input) (Real Gas, ft/sec)	
RBD(K,M)	r, Local nose radius at axial station K and meridional surface M; maximum value of K = 25, maximum value of M = 8	
RC	Corner radius for biconic nosetip geometry	
RF(I)	Array of radii of conical frustum segments (NCON + 1 values)	
RIDEAL	R, Gas constant (Ideal Gas)	(1.0)
RN	r_N, Nose radius (spherical or biconic noses)	
STAB	Stability factor on CFL condition for supersonic calculations	(1.0)
TEST(11)	Convergence criterion for shock property calculations (Real Gas)	(10^{-4})
TEST(12)	Convergence criterion for stagnation condition iteration (Real Gas)	(10^{-4})
TEST(28)	Test for initiation of bow and embedded shock intersection procedure; shock intersection assumed when $(y_{s_1}-y_{s_2})/(y_{s_1}) \leq$ TEST(28)	(0.05)

TEST(29)	Convergence criterion for embedded and bow shock intersection iterative calculation	(0.001)
TEST(30)	Test for initiation of flare calculation; flare assumed when THF(I + 1) - THF(I) > TEST(30), in degrees	(2.0)
TEST(31)	Convergence criterion for global transonic iteration	(0.005)
TEST(32)	Damping factor for global transonic iteration	(0.6)
TEST(33)	Convergence criterion for local transonic iteration	(0.005)
TEST(34)	Convergence criterion for supersonic shock calculation	(10^{-5})
TEST(35)	Alternate convergence criterion for supersonic shock calculation	(10^{-4})
TEST(36)	Acceleration factor for local transonic iteration	(1.1)
TEST(37)	Convergence criterion for flare embedded shock initialization iteration	(10^{-4})
TEST(38)	Increment in axial location used in initializing embedded shock calculation	(0.05)
TEST(39)	Criterion for respacing grid points in region between embedded and bow shocks	(0.05)
TEST(40)	Criterion for respacing grid points in region between body and embedded shock	(0.05)
THF(I)	Array of cone angles of conical frustum segments (degrees) (NCON values)	
THN	Nose cone angle for biconic nosetips	
TINF	T_∞, Freestream static temperature (Real Gas, ^oR)	(1.0)
XBAR,YBAR, ZBAR	$(\overline{X},\overline{Y},\overline{Z})$ Moment reference point	
ZBD(K)	Axial stations for specification of nose geometry, maximum value of K = 25	
ZF(I)	Array of axial stations of conical frustum segments (NCON + 1 values)	
ZIDEAL	z, Compressibility factor (Ideal Gas)	(1.0)

DISTRIBUTION LIST

Ballistic Missile Office
BMO/SYDT
Attn: Maj. K. Yelmgren (2)
Norton AFB, CA 92409

Defense Technical Information Center (2)
Cameron Station
Alexandria, VA 22314

Air University Library
Maxwell AFB, AL 36112

TRW DSSG
Attn: W. Grabowsky (2)
P. O. Box 1310
San Bernardino, CA 92402

TRW Systems Group (2)
Attn: J. Ohrenberger
M. Gyetvay
1 Space Park
Redondo Beach, CA 92078

Headquarters, Arnold Engineering
Development Center
Arnold Air Force Station
Attn: Library/Documents
Tullahoma, TN 37389

Armament Development and Test Center
Attn: Technical Library, DLOSL
Eglin AFB, FL 32542

Air Force Wright Aeronautical Laboratories (3)
Air Force Systems Command
Attn: M. Buck (AFWAL/FIM)
R. Neumann (AFWAL/FIMG)
V. Dahlem (AFWAL/FIMG)
Wright-Patterson AFB, OH 45433

U. S. Army Ballistic Missile
Defense Agency/ATC-M
Attn: J. Papadopoulos
P. O. Box 1500
Huntsville, AL 35807

Director, Defense Nuclear Agency
Attn: J. Somers (SPAS)
Washington, DC 20305

Naval Surface Weapons Center
Attn: Carson Lyons/K06
White Oak Laboratories
Silver Spring, MD 20910

Acurex Aerotherm
Aerospace Systems Division
Attn: C. Nardo
485 Clyde Avenue
Mountain View, CA 94042

Avco Systems Division
Attn: N. Thyson
201 Lowell Street
Wilmington, Mass 01887

General Electric Company
Attn: R. Neff
3198 Chestnut Street
Philadelphia, PA 19101

Lockheed Missiles and Space Co.
P. O. Box 504
Attn: G. T. Chrusciel
Sunnyvale, CA 94086

McDonnell Douglas Astronautics Co.
Attn: J. Copper
5301 Bolsa Avenue
Huntington Beach, CA 92647

PDA Engineering
Attn: M. Sherman
1560 Brookhollow Drive
Santa Ana, CA 92705

Sandia Laboratories
P. O. Box 5800
Attn: Library
Albuquerque, NM 87115

Science Applications, Inc.
Attn: A. Martellucci
994 Old Eagle School Road
Suite 1018
Wayne, PA 19087